A Thermodynamic Model for the Shape and Stability of Twinned Nanostructures

A. S. Barnard[†]

Department of Materials, University of Oxford, Parks Road, Oxford, OX1 3PH, United Kingdom

Received: September 5, 2006; In Final Form: September 28, 2006

Although thermodynamically metastable, planar defects are often observed in many faceted nanomaterials including nanocrystals, nanorods, and nanowires, even after annealing. These planar defects include contact twins and (intrinsic or extrinsic) stacking faults, and are usually neglected by most analytical models. For example, many bulk metals have the face-centered cubic structure, but small nanocrystals and nanorods of the same material often exhibit various structural and morphological modifications such as single or multiple symmetric twinning, as well as 5-fold cyclic twinning resulting in decahedral and truncated decahedral nanostructures. Presented here is a general analytical model for the investigation of nanomaterials of arbitrary shape, and with any configuration of planar defects. The model is tested for the case of twinning in unsupported gold nanocrystals and nanorods, and is shown to give results in excellent agreement with experimental and computational studies reported in the literature.

1. Introduction

It has been widely shown that many fundamental properties of nanomaterials have a strong dependence on particle size, or have no macroscopic analogue.[1,2] In recent times nanomorphology (that is, the structure, shape, and phase of nanomaterials) is also being found to be critically important to many of the properties.[3,4] An obvious example is in the field of nanocatalysis,[5−7] but shape dependence has also been observed in the elastic properties of nanorods,[8] optical and electronic properties of quantum dots (such as luminescent properties),[9,10] and quantum confinement effects.[11] When examining the shapes of various types of nanostructures, theory and simulation is proving to be a very useful tool, with both analytical and computational models providing valuable explanatory and predictive capabilities to complement and guide experimentation.[12]

However, real nanocrystals are not always "crystallographically ideal", and may contain imperfections that are usually neglected by most models. These imperfections include (but are not limited to) planar defects such as contact twins and intrinsic or extrinsic stacking faults, which readily form during crystal growth in materials with low stacking fault or twin boundary energy, and surface energy anisotropy.[13] In particular, although many bulk metals have the face-centered cubic (fcc) structure, nanocrystals and nanorods of the same material often exhibit various structural and morphological modifications such as single or multiple symmetric twinning,[5,14−16] and cyclic twinning resulting in decahedral[17] and truncated decahedral structures.[18−20] Figure 1 shows transmission electron micrographs of these different types of twinning in gold nanocrystals, along with structural representations of each type, highlighting the location of the twin planes and the surface re-entrant angles. The observation of decahedral structures, often referred to as multiply twinned particles or MTPs (see Figure 1b) has attracted considerable attention, due to their unusual, crystallographically forbidden 5-fold (pentagonal) symmetry. Some examples of nanocrystals and nanorods that have exhibited multiply twinned 5-fold structures include copper,[21] silver,[22−26] platinum,[5,6,27] and
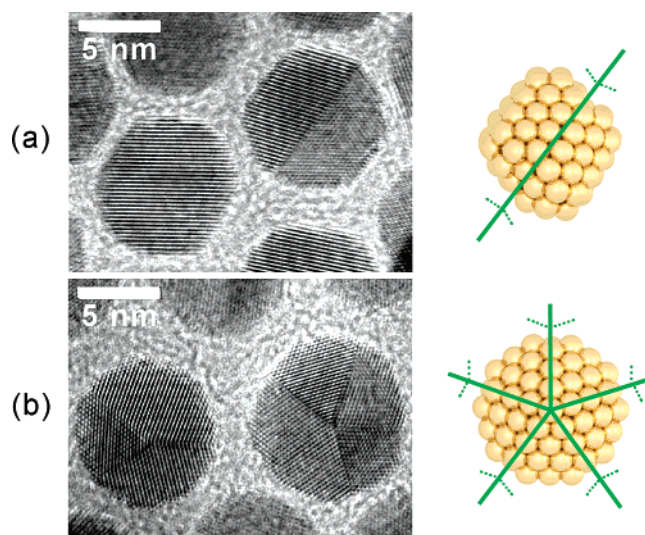
Figure 1. Transmission electron micrographs showing examples of twinning in gold nanoparticles, courtesy of Xiao-Min Lin from Argonne National Laboratory. Examples include (a) an un-twinned (pristine) nanoparticle (left) and a nanoparticle with a single symmetric twin in a {111} plane (right) and (b) two decahedral nanoparticles showing cyclic 5-fold twinning. Structural representations of each type of twinning are also given to the far right, with the location of the twin planes highlighted by solid lines, and the location of the re-entrant angles highlighted by dotted lines.

gold.[8,28−30] Of these, gold is arguably the most extensively characterized, including an impressive number of computational studies over a range of length scales.[14,31−51]

In addition to these studies of metal particles, similar structures have been shown to form spontaneously during computer simulations of a hard sphere system (being the simplest nontrivial model of a liquid). Although hard sphere systems are known to form face-centered cubic close-packed structures as the stable crystalline phase, small nuclei exhibited a predominance of multiply twinned and decahedral structures.[52] This suggests that the formation of stacking faults, planar contact twins, and cyclic twinning is a fundamental phenomena in

---

† E-mail: amanda.barnard@materials.ox.ac.uk.

Shape and Stability of Twinned Nanostructures

J. Phys. Chem. B, Vol. 110, No. 48, 2006 **24499**

nanosized particles that should not be omitted in any rigorous energetic description.

Rather than treating each type of shape and structure explicitly, via individual computer simulations, another approach to the examination of the shape of these nanostructures is based on the Wulff construction.[53] The Wulff construction describes the equilibrium shape of crystals, given by the convex envelope of planes (perpendicular to the surface normals) that minimizes the total surface energy for a given enclosed volume. Equivalently, the distance of a surface plane from the center-of-mass of the crystal is proportional to the surface energy of that plane. This approach was first applied to twinning in metal nanocrystals by Ino,[17] who calculated the free energy of tetrahedral, truncated octahedral, icosahedral, and decahedral nanocrystals using macroscopic quantities such as cohesive, surface, twin-boundary, and elastic strain energies. In addition to this, Ino proposed a truncated decahedron (thereafter referred to as the "Ino decahedron" in the literature), which involved exposing higher energy (100) facets, but lowered to total surface-to-volume ratio. This shape was shown to be lower in energy than a simple decahedron, but was not found to be a low energy shape in general. Ino found that in the case of gold nanocrystals, particles smaller than ∼10 nm in diameter are likely to be icosahedral, beyond which the optimal structures are truncated octahedra. It was concluded that neither the simple decahedron nor the Ino decahedron were structurally preferred at any size.[17,54]

Following in this vein, the stability of decahedral particles was revisited by Marks,[18,19] who devised a modification to the Ino decahedron that allowed for re-entrant facets at the twin boundaries of the decahedron (in the directions corresponding to the decahedral unit's (111) twinning planes, ignoring strain). This resulted in a nonconvex polyhedron more in keeping with experimental observations, while also being consistent with the ideal of a Wulff shape. This structure has since been referred to as the "Marks decahedron" in the literature. Using this shape, Marks predicted the evolution in nanomorphology with increasing nanocrystal size to progress from icosahedral to decahedral to truncated octahedral shapes. At a critical size, the Marks decahedron becomes energetically more favorable than an icosahedron (of equivalent volume) before the pristine fcc Wulff shape dominates at large sizes.[19] The energetic crossovers between these structures have also been explicitly examined and this energetic order of morphologies confirmed by Baletto et al.[46,55]

The advantages of this type of thermodynamic modeling include the ability to compare nonequilibrium shapes, to optimize the morphology with respect to experimentally relevant parameters such as size, temperature, or surface chemistry (or chemical potential), and to consider with relative ease nanoparticles at sizes traditionally inaccessible to all but atomistic level simulations.[56] However, to examine a wider range of realistic nanostructures, it is desirable to have a general expression that incorporates the approach to twinning (and stacking faults) outlined above into existing analytical theories of nanomorphology. This would facilitate the examination of twinning in nanomaterials of any shape (including nanocrystal, nanorods, and nanowires), without necessitating a large number of explicit simulations of individual structures. In addition to this, such a model would be able to investigate hypothetical twinning configurations that are not observed experimentally, and compare the relative stability of these and other metastable shapes and structures.

This is the aim of the present work, which will begin by reviewing the thermodynamic formalism of the previously

reported[56] multiscale shape-dependent theoretical model for unsupported, pristine (un-twinned) nanostructures, and then present new terms to describe planar defects and the associated edges at re-entrant angles. The new term will be derived in a manner consistent with the existing model, and will take as input quantities that may be readily calculated using accurate first principles methods. This will be followed by a discussion of practical implementation of the model, and results of its application to a test system, in this case, twinning in unsupported gold nanocrystals and nanorods.

2. Theoretical Formalism

As indicated above, a general shape-dependent thermodynamic model for nanostructures has already been derived for the case of defect-free, pure nanocrystals and reported in ref 56. It is based on a summation of the Gibbs free energy $G_x(T)$ of a nanoparticle of material in phase x, and includes contributions from the bulk and surface of the structure, as well as from the edges and the corners. To extend this treatment to include planar defects such as twin planes or stacking faults, this will now become the sum of contributions from the particle bulk, surfaces, edges, corners, and planar defects such that:

$$G_x(T) = G_x^{\text{bulk}}(T) + G_x^{\text{surface}}(T) + G_x^{\text{edge}}(T) + G_x^{\text{corner}}(T) + G_x^{\text{pd}}(T) + \dots \quad (1)$$

In the case of defect-free nanostructures $G_x^{\text{bulk}}(T)$, $G_x^{\text{surface}}(T)$, $G_x^{\text{edge}}(T)$, and $G_x^{\text{corner}}(T)$ are the zeroth-order, first-order, second-order, and third-order terms in the Gibbs free energy expansion, respectively. $G_x^{\text{pd}}(T)$ is the first higher order perturbation to be included, although one can also think of others that are not included, such as lattice vacancy point-defects.

2.1. Summary of Defect-Free Terms. The zeroth-order term, $G_x^{\text{bulk}}(T)$, is defined as the standard free energy of formation $\Delta G_x(T)$, which depends on the temperature T. The first-order term, $G_x^{\text{surface}}(T)$, is expressed in terms of the molar mass M and density ρ_x of the material in a phase x, and the surface-to-volume ratio q:

$$G_x^{\text{surface}}(T) = \frac{M}{\rho_x} q \sum_i f_i \gamma_{xi}(T) \quad (2)$$

where $\gamma_{xi}(T)$ is the surface free energy of facet i. Similarly, the energy associated with an edge $G_x^{\text{edge}}(T)$ is expressed as the sum of the edge free energy λ_{xj} of the edges j, and the edge-to-volume ratio p,

$$G_x^{\text{edge}}(T) = \frac{M}{\rho_x} p \sum_j g_j \lambda_{xj}(T) \quad (3)$$

and the energy associated with a corner $G_x^{\text{corner}}(T)$ may be expressed in terms of the corner free energy ϵ_x of corners k along with the corner-to-volume ratio w such that

$$G_x^{\text{corner}}(T) = \frac{M}{\rho_x} w \sum_k h_k \epsilon_{xk}(T) \quad (4)$$

In each case the weighting factors are defined so that

$$\sum_i f_i = \sum_j g_j = \sum_k h_k = 1 \quad (5)$$

These weighting factors, along with the ratios q, p, and w, are determined geometrically for each shape and the facets therein.

24500 *J. Phys. Chem. B, Vol. 110, No. 48, 2006*

Barnard

The full derivation of this part of the model, along with the introduction of the volume dilation e due to isotropic surface stress, is outlined in detail in ref 56, and given by eq 6

$$G_x^{\text{pristine}}(T) = \Delta G_x(T) + \frac{M}{\rho_x}(1 - e)[q\sum_i f_i\gamma_{xi}(T) + p\sum_j g_j\lambda_{xj}(T) + w\sum_k h_k\epsilon_{xk}(T)] \quad (6)$$

In this model the shape dependence is introduced by ratios q and p and w, as well as the weighted sums of the surface energies and the isotropic surface stresses, corresponding to the surfaces present in the particular morphology of interest. The size dependence is introduced by the ratios q, p, and w and by the reduction of e as the crystal grows larger.

As discussed in ref 56, although the overall affect of e is small, inclusion of this term is particularly important, since it has been reported experimentally that small nanoparticles typically exhibit a lattice contraction, resulting in lattice parameters smaller than that of their bulk counterpart.[58] It has previously been shown that the Laplace−Young equation is suitable for approximating the volume dilation of faceted nanoparticles.[56] This dilation includes the bulk modulus B_0, and is defined as

$$e = \frac{2\sum_i f_i\sigma_{xi}}{B_0R} \quad (7)$$

where σ_{xi} is the surface stress of the particular crystallographic surface i. This model has already been shown to provide an excellent description of the shape of metals,[59] oxides,[60,61] and semiconductors,[56,62] in comparison with experiment. It is also worth pointing out that e may also be define so as to include contributions from external pressure P_{ex}, such that

$$e_{\text{total}} = \frac{2\sum_i f_i\sigma_{xi}}{B_0R} + \frac{P_{\text{ex}}}{B_0} \quad (8)$$

2.2. Thermodynamic Contributions from Planar Defects. However, the aim here is to extend this model beyond the consideration of perfect crystals, and to include a complementary term for the Gibbs free energy of a planar defect $G_x^{\text{pd}}(T)$, as indicated in eq 1. As mentioned above, it is mandatory that such a term is consistent with the preceding terms and is able to describe single and multiple symmetrically twinned particles (rods and wires), and structures with cyclic twinning with equal accuracy.

When considering a twin plane there are two important energetic contributions that must be included. These are the free energy of the planes $G_x^{\text{tp}}(T)$, and the free energy associated with the re-entrant angles intersecting with the surfaces of the nanostructure $G_x^{\text{lt}}(T)$:

$$G_x^{\text{pd}}(T) = G_x^{\text{tp}}(T) + G_x^{\text{lt}}(T) \quad (9)$$

Since these are analogous to the $G_x^{\text{surface}}(T)$ and $G_x^{\text{edge}}(T)$ terms,[63] respectively, it naturally follows that $G_x^{\text{tp}}(T)$ be expressed as a product of free energy of a particular defect plane $\nu_{x\theta}(T)$ in the crystallographic orientation θ, and the area of that plane a_θ.

$$G_x^{\text{tp}}(T) = \sum_\theta a_\theta\nu_{x\theta}(T) \quad (10)$$

Further, the free energy of the edges along the re-entrant angles $G_x^{\text{lt}}(T)$ is expressed as a product of the re-entrant *line tension* $\eta_{x\phi}(T)$ along the direction ϕ and the length of the re-entrant edge $l_{\theta\phi}$ forming part of the circumference of the defect plane in orientation θ. If we were considering a stacking fault (as opposed to a twin plane), then $\eta_{x\phi}(T)$ would describe the energy of the steps intersecting with the surfaces along ϕ.

$$G_x^{\text{lt}}(T) = \sum_\phi l_{\theta\phi}\eta_{x\phi}(T) \quad (11)$$

It is important to note here that the re-entrant line tension $\eta_{x\phi}(T)$ describes concave or convex edges at re-entrant angles. Although some re-entrant edges may intersect with conventional edges of the nanostructure described by $\lambda_{xj}(T)$ in eq 3, the energy of $\lambda_{xj}(T)$ in the presence of a re-entrant angle will differ from that in the absence of a re-entrant angle. The combination of $\lambda_{xj}(T)$ and $\eta_{x\phi}(T)$ will describe the total energy of the edge in this case, but the components should still be included separately as shown here if the model is to describe defective and pristine nanostructures with equal accuracy.

Therefore, the free energy for a planar defect in a material of phase x may be written as:

$$G_x^{\text{pd}}(T) = \sum_\theta[a_\theta\nu_{x\theta}(T) + \sum_\phi l_{\theta\phi}\eta_{x\phi}(T)] \quad (12)$$

For consistency, this is in turn written in terms of M and ρ_x, by introducing the number density of planar defects $n = n_t/V$ (where n_t is the total number of planar defects in the nanostructure, and V is the total volume of the nanostructure), so that eq 1 may now be written as:

$$G_x(T) = \Delta G_x(T) + \frac{M}{\rho_x}(1 - e)[q\sum_i f_i\gamma_{xi}(T) + p\sum_j g_j\lambda_{xj}(T) + w\sum_k h_k\epsilon_{xk}(T) + n\sum_\theta(a_\theta\nu_{x\theta}(T) + \sum_\phi l_{\theta\phi}\eta_{x\phi}(T))] \quad (13)$$

This provides a general model for arbitrary nanostructures containing n_t planar defects that may be solved for any desired size or shape.

However, we can see that (although theoretically simple) there is one major issue that will complicate and possibly inhibit the implementation of this model in practice. There are a relatively large number of terms that must be calculated to parametrize the model, especially if realistic polyhedral nanostructures are to be considered. These include $\gamma_{xi}(T)$, $\lambda_{xj}(T)$, $\epsilon_{xk}(T)$, $\sigma_{xi}(T)$, $\nu_{x\theta}(T)$, and $\eta_{x\phi}(T)$, which must be calculated explicitly for all i, j, k, θ, and ϕ of interest. Each will depend on the crystallographic orientation of the surfaces, the combinations of surfaces intersecting at the edges and corners, the orientation of the planar defects, and the properties of the material x. It is also of great importance that the same computational method be used for all $\gamma_{xi}(T)$, $\lambda_{xj}(T)$, $\epsilon_{xk}(T)$, $\sigma_{xi}(T)$, $\nu_{x\theta}(T)$, and $\eta_{x\phi}(T)$, and to the same convergence criteria, so that energetic differences can reliably be attributed to materials properties and not to numerical inconsistencies.

Although these values can be calculated in a relatively straightforward manner when $T = 0$ (making G_x equivalent to the enthalpy of formation H_x), the number of individual values required makes parametrization of this model rather computationally intensive. Therefore, to address these issues, the following sections have been given over to discussing ways of

Shape and Stability of Twinned Nanostructures

J. Phys. Chem. B, Vol. 110, No. 48, 2006 **24501**

simplifying implementation, and to testing the model.

3. Practical Implementation and Ranges of Applicability

The most convenient way of making this model more practical is via appropriate truncation. That is, to decide which terms may be omitted, which must be included for a given situation. Truncation of the model in this way will also require quantification of the consequential effective size range to which it may be reliably applied.

In practice the calculation of all j edges and k corners can prove as computationally intensive as explicitly calculating the optimized geometry of complete, isolated nanostructures. Furthermore, the importance of λ_{xj} and ϵ_{xk} in the total free energy of the system is largely unknown. On the basis of the construction of the model we can see that while $G_x^{\text{surface}} \propto 1/R$, $G_x^{\text{edge}} \propto 1/R^2$, and $G_x^{\text{corner}} \propto 1/R^3$. This follows directly from the definition of q, p, and w, and indicates that the contribution from the surfaces will dominate above a "critical size" that is to some degree independent of material x. This issue has previously been examined for C, Si, and Ge nanocrystals, where estimates for edge free energies based on step energies produced total edge energies (for crystals containing 10^3 to 10^6 atoms) that are 1 to 3 orders of magnitude smaller than the total energies for the adjacent surfaces, as described in ref 56. In this study it was shown that the total contribution from the edges and corners is considerably smaller than the contribution from the surfaces for the sizes larger than $\sim 10^4$ atoms. Therefore, it is reasonable to assume that edge and corner energies will have limited significance for nanocrystals larger than this size, usually denoted by a diameter D. When considering nanostructures with a diameter less than D it is still preferable to examine each morphology explicitly, by undertaking suitable calculations of isolated structures (using ab initio or tight-binding methods). The precise value of D depends on the material, but as a general rule of thumb $D \approx [((6 \times 10^4)V)/4\pi N]^{1/3}$, where N is the number of atoms in the unit cell and V is total volume of the unit cell.

Similarly, at large sizes, in the range of 75–100 nm in diameter, the contribution to the total free energy from surfaces is many orders of magnitude smaller than the contribution from the bulk.[57] This indicates that the energetics of the surface is less significant, and other bulk effects more significant. In this size regime, for example, the macroscopic (bulk) strain is as important as the surface strain, and the bulk entropy will be as important as the surface entropy. The present model does include the bulk strain, but only includes other macroscopic thermodynamic variables such as vibrational entropy if they are explicitly included in ΔG_x^{o} in the standard way. This consequently imposes an upper (size) limit for which accuracy may be assured, for example, when ΔG_x^{o} is omitted and the free energy is described only *with respect to bulk*.

For the purposes of studying nanocrystals with planar defects a truncated version of the model is given, where the energetic contribution from edges and corners are ignored. This provides an *approximate* value, G_x^{approx}, which is a sum of contributions from the bulk and surfaces and planar defects of the nanostructure, such that (at ($T = 0$))

$$G_x^{\text{approx}} = \Delta G_x^{\text{o}} + \frac{M}{\rho_x}(1 - e)[q\sum_i f_i \gamma_{xi} + n\sum_\theta (a_\theta \nu_{x\theta} + \sum_\phi l_{\theta\phi}\eta_{x\phi})] \quad (14)$$

With use of this truncated version, G_x^{approx} may be expected to give a good approximation of the total free energy at sizes within the *range of applicability* between D and ~ 100 nm. This range of applicability has also been discussed previously in refs 56 and 57, and provides the size range of the structures in which uncertainties in the total free energy due to particle geometry are minimized. We can see that G_x^{approx} is significantly less computationally intensive than the full version, as it only requires explicit determination of the values of γ_{xi} and σ_{xi} for all orientations i of interest (along with the bulk modulus B_0), in addition to the energy of the planar defects $\nu_{x\theta}$ and associated line tensions $\eta_{x\phi}$. In some cases the effect of σ_{xi} may be small and e may also be omitted, but this should be tested for each system under consideration. The question remains as to how important the inclusion of $\eta_{x\phi}$ will be with respect to $\nu_{x\theta}$. To investigate this question and test the formalism, in the following section the new shape-dependent model for nanostructures containing planar defects is applied to gold nanocrystals and nanorods.

4. Application to Gold Nanostructures

Gold nanostructures are an excellent test system for use here, since a variety of types of twinning have been observed in both nanocrystals and nanorods, and have been studied in some detail by other authors both computationally and experimentally.

Previously the surface free energies γ_{xi} and isotropic surface stresses σ_{xi} of reconstructed {111} and {100} gold surfaces have been calculated, using fully relaxed periodic slabs with 2×2 (surface) super-cells, and nine and eight atomic layers perpendicular to the desired surface, respectively.[59] These values, along with the bulk modulus B_0, were calculated by using scalar relativistic density functional theory (DFT) within the generalized-gradient approximation (GGA), and the final values of $B_0 = 157 \pm 1.9$ GPa, $\gamma_{\text{Au}(111)} = 84$ meV/Å^2, $\sigma_{\text{Au}(111)} = 174$ meV/Å^2, $\gamma_{\text{Au}(100)} = 97$ meV/Å^2, and $\sigma_{\text{Au}(100)} = 188$ meV/Å^2 have been shown to be in excellent agreement with other theoretical studies and experimental results where available. Using the same computational method and convergence as used in ref 59 the energy of a {111} twin plane has been calculated. This has been done in a straightforward manner analogous to the calculation of the surface free energy, using a 1×1 bulk super-cell 24 atomic layers thick (oriented with the ⟨111⟩ direction along the z-axis), with two twin planes introduced in the x−y plane. The final value of $\nu_{\text{Au}(111)} = 1.7$ meV/Å^2 is in very good agreement with the value of 1.6 meV/Å^2 calculated by Rosengaard and Skriver using the LMTO-ASA method,[64] and the value of 1.3 meV/Å^2 calculated by Crampin et al.[65] using the supercell-pseudopotential method, and Schweizer et al.[66] using the LKKR method, as well as the experimental value of 0.9 meV/Å^2 obtained by Murr.[67]

Obtaining values for re-entrant line tensions is not so straightforward. These were determined by fitting to the results for the set of decahedrons (Au$_{75}$, Au$_{101}$, and Au$_{146}$) reported in ref 51, which (again) were calculated with the same computational procedure used for all of the values for B_0, γ, σ, and ν listed above. Fitting to these particles gave the values of $\eta_{\text{Au}||(111)} = -0.54$ eV/Å and $\eta_{\text{Au}||(100)} = -0.40$ eV/Å, and while not the ideal way of calculating the re-entrant line tensions, it is sufficient to test the model above. It is interesting that the values are negative, however, since no previously reported values could be found for comparison, the accuracy of these $\eta_{x\phi}$ will be best assessed by considering final results described in the following sections.

Although it is obvious that twin planes must be accompanied by re-entrant angles where the planes intersect with free surfaces
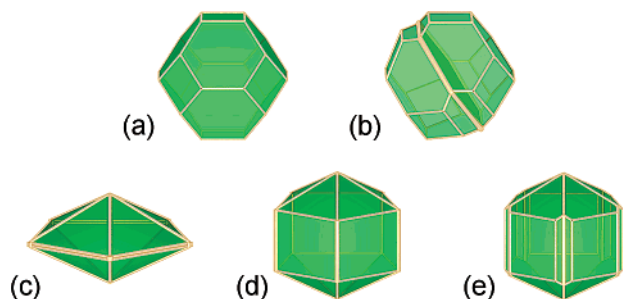
Figure 2. Schematic representations of gold nanocrystals without twinning (a), with a single symmetric (111) twin plane (b), and with 5-fold cyclic twinning in the simple decahedron (c), Ino decahedron (d), and Marks decahedron configurations (e).
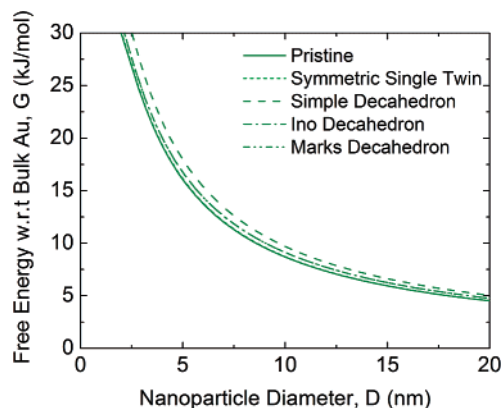

Figure 3. The approximate free energy G_x^{approx} of gold nanoparticles (with respect to bulk Au) for shapes corresponding to the pristine truncated octahedron, symmetrically twinned truncated octahedron, simple decahedron, Ino decahedron, and Marks decahedron (as shown in Figure 2), calculated with eq 14.

(and that certain configurations of a re-entrant angle will minimize the total energy of the planar defect), if we think about the physical consequences of negative line tensions it means that these particular configurations will actually stabilize the defect. Furthermore, if the endothermic contribution to the total free energy from the twin boundary plane is compensated by an exothermic contribution from the line tension of the circumference, then (depending on the size of the structure) the planar defect may be energetically preferred over a pristine structure.

Before proceeding it is also important to point out that, although the model outlined here is valid at any temperature (and pressure, as indicated by eq 8), the following testing procedure uses values of each input parameter calculated at $T = 0$ and with $P_{\text{ex}} = 0$. Therefore, in terms of materials properties, the following results correspond to the minimum energy structures of gold at 0 K and in an absolute vacuum. So as not to complicate the testing procedure, consideration of more realistic atmospheric conditions has been reserved for future work.

4.1. Gold Nanocrystals. As the first test, the truncated version of the model has been used to calculate the approximate free energy of formation for pristine and twinned gold nanocrystals. Schematic representations of the model shapes are shown in Figure 2. In this figure the pristine (un-twinned) fcc structure and the same fcc structure with a single symmetric twin are illustrated in parts a and b, respectively. The pristine particle is a truncated octahedron, identified as the lowest energy shape for fcc gold nanocrystals larger than ∼4 nm, at $T = 0$,[59] and the singly twinned shape is obtained by rotating half of the truncated octahedron 180° around a [111] axis. In contrast, the 5-fold simple decahedron, Ino decahedron, and Marks decahedron, all containing five twin planes in a cyclic configuration, are illustrated in Figure 2, parts c, d, and e, respectively. The simple decahedron is a pentagonal dipyramid, and the 10 faces are equilateral triangles. The Ino decahedron is a pentagonal dipyramid truncated in the lateral ⟨100⟩ directions at a distance corresponding to the Wulff construction, creating a pentagonal prism between the pyramids. As mentioned above, this truncation serves to lower the total surface-to-volume ratio. The Marks decahedron may be considered as a modified Ino decahedron, with new nonconvex facets added in the directions corresponding to the decahedral unit's (111) twinning planes, creating re-entrant facets along the edges of the pentagonal prism.

By using eq 14 and the list of parameters calculated with the relativistic density functional theory reported above, G_x^{approx} has been calculated for each of the shapes in Figure 2. These results are shown in Figure 3, where we can see that the Marks decahedron (shown in Figures 1b and 2e) is considerably lower in energy than the other shapes at small sizes. There are a
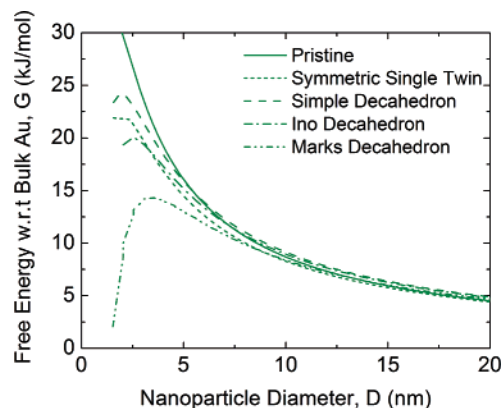
number of crossing points in this graph (although some are difficult to discern), but the evolution in nanomorphology with increasing size predicted by this model is the following: Marks decahedron ≤ ∼9.5 nm ≤ single symmetrical twinned fcc truncated octahedron ≤ ∼61 nm ≤ pristine fcc truncated octahedron. If the single symmetrical twinned fcc truncated octahedron were ignored, the model predicts a crossover between the Marks decahedron and the pristine fcc truncated octahedron at ∼13.5 nm (although the plots are very shallow at this point). In addition to this the model predicts that the pristine fcc truncated octahedron is the least favored structure below ∼5.6 nm, and although the Ino decahedron is always lower in free energy than the simple decahedron, it is never the energetically preferred shape, in full agreement with the original results of Ino[54] and Marks.[18] At the larger sizes (beyond the range plotted in Figure 3, ≳21 nm) the difference in energy between the pristine truncated octahedron and the single symmetrical twinned structure is within the uncertainties of the model, effectively making this a thermodynamic coexistence region at this level of approximation. Formation of one structure or the other in this range will therefore be determined by kinetics. It is also worth mentioning that at exceedingly large sizes (beyond the effective range of applicability) the model clearly predicts the pristine structure to be the thermodynamic ground state.

To investigate the question as to how important the inclusion of $\eta_{x\phi}$ will be with respect to $\nu_{x\theta}$, G_x^{approx} has been calculated for each of the shapes in Figure 2 by using eq 14 but with $G_x^{\text{lt}} = 0$. These results are shown in Figure 4, where (as one would expect) the results for the Ino decahedron and the Marks decahedron are coincident, and the difference in energy between the pristine truncated octahedron and the single symmetrical twinned structure is less than the uncertainties of the model. We can see that when $\eta_{x\phi}$ is omitted none of the decahedrons are energetically preferred at any size, indicating that the $\eta_{x\phi}$ must be included if the model is to reproduce results in agreement with experiment[32,30,59,68] and the results of explicit computational studies.[32−34,44,45,55,69]

The importance of the inclusion of re-entrant edges has been previously examined by a number of computational studies with isolated particles of different sizes. For example, an extensive study by Cleveland et al.[33,34,37] using many-body embedded-atom potential and fully relaxed structures with icosahedral, decahedral, and pristine fcc morphologies between 50 and 5000 atoms (≲6 nm) clearly showed the energetic preference of the

Shape and Stability of Twinned Nanostructures

J. Phys. Chem. B, Vol. 110, No. 48, 2006 **24503**

Figure 4. The approximate free energy G_x^{approx} of gold nanoparticles for shapes corresponding to the pristine truncated octahedron, symmetrically twinned truncated octahedron, simple decahedron, Ino decahedron, and Marks decahedron, calculated with eq 14 with $\eta_{x\phi} = 0$.
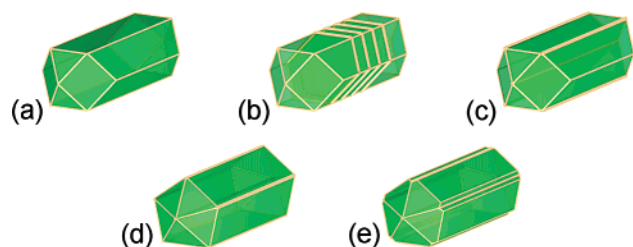

Figure 5. Schematic representations of gold nanorods without twinning (a), with four lateral symmetric (111) twin planes (b), with four hypothetical longitudinal (111) twin planes (c), and finally with longitudinal 5-fold cyclic twinning in the simple decahedral (d) and Marks decahedral configurations (e).

Marks decahedron over the Ino decahedron and the pristine fcc truncated octahedron in this range. This re-entrant angle has also been shown to be important in other metallic nanostructures, such as the silver nanoparticles examined by Baletto et al.[70]

4.2. Gold Nanorods. Another important goal of the present work is that the new model be applicable to defective nanomaterials of any shape, including nanorods and nanowires, and that it enable the investigation of hypothetical twinning configurations that are not observed experimentally. Therefore, as the second test, eq 14 and the parameters listed at the beginning of section 4 have been used to calculate the approximate free energy of formation for pristine and twinned gold nanorods. Schematic representations of the model shapes are shown in Figure 5. In this figure a pristine (un-twinned) cuboctahedral fcc nanorod and the same nanorod with four lateral symmetric twins are illustrated in Figure 5, parts a and b, respectively. In addition to this, a hypothetical twinning configuration is included for this cuboctahedral fcc nanorod with four longitudinal (111) twin planes, as shown in Figure 5c. Finally, two 5-fold decahedral nanorods are included, corresponding to the nanorod version of the simple (or Ino) decahedron and Marks decahedron, as shown in Figure 5, parts d and e, respectively.

The results of the approximate free energy for these gold nanorods are shown in Figure 6, as a function of the nanorod aspect ratio, α. These calculations are all volume conserving (with the total number of atoms $N_{\text{Au}} = 10\,000$), so that both the diameter and length change as α is varied. We can see that the Marks decahedral nanorod (shown in Figure 5e) is the lowest energy nanorod, and that the energetic preference of this morphology over the alternatives increases with increasing α. It is also clear that, at $N_{\text{Au}} = 10\,000$, the pristine nanorod is the least favorable, indicating that gold nanorods would prefer to
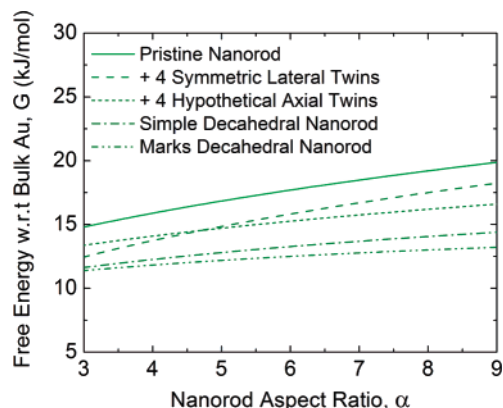
Figure 6. The approximate free energy G_x^{approx} of gold nanorods (with respect to bulk Au) calculated with eq 14 for shapes corresponding to the pristine cuboctahedral nanorod, the cuboctahedral nanorod with four lateral (111) twin planes, the cuboctahedral nanorod with four hypothetical longitudinal (111) twin planes, the simple decahedral nanorod, and the Marks decahedral nanorod (as shown in Figure 5).

be twinned rather than adopt this (pristine) shape. However, the type of twinning that the model predicts for the cuboctahedral nanorod depends on α, with lateral twinning being preferred below $\alpha \approx 4.7$ and the hypothetical longitudinal twinning being preferred over this range. While it is unlikely that this hypothetical twinning configuration will be observed, due to the considerable energetic preference for 5-fold decahedral twinning at higher aspect ratios, it is an indication that longitudinal twinning will certainly be more favorable in high aspect gold nanowires than lateral twinning.

In general, the prediction that longitudinal twinning is the preferred configuration for gold nanorods is in excellent agreement with the experimental observations of Canizal et al.,[29] who concluded that gold nanorods either exhibit parallel (longitudinal) bands of twin planes or concentric (5-fold) twins forming pentagonal nanorods, growing along the $\langle 112 \rangle$ direction. Similarly, Johnson et al.[71] and Jana et al.[72] observed similar results for nanorods of different aspect ratios (which can be easily moderated with surfactants[73,74]).

5. Conclusion

Presented is an extension of a shape-dependent thermodynamic model to include any configuration of planar defects in unsupported nanostructures. The new term describing planar defects has been derived in a manner consistent with the defect-free terms, and takes as input quantities that may be easily calculated by using first principles methods. In addition to this, an approach to practical implementation has been discussed, and the effective range of applicability of the model outlined for a more convenient, truncated version.

The model has also been tested for the case of gold nanocrystals and nanorods, examining the relative stability of different configurations of symmetric (111) twins, cyclic 5-fold (decahedral) twins, and a hypothetical 4-fold cyclic twinned nanorod. The results of these tests are in excellent agreement with experimental observations and explicit computational studies reported in the literature, showing that the evolution of morphologies in gold nanocrystals is the following: Marks decahedron, symmetrically twinning truncated octahedron, and then pristine truncated octahedron (among the shapes considered). The new model also predicts that higher aspect gold nanorods show a definite preference for longitudinal twinning and the formation of pentagonal nanostructures, in agreement with experimental studies. It is hoped that this model will find

use in the investigation of planar defects and cyclic twinning in other nanomaterials, such as aluminum, copper, silver, and platinum.

References and Notes

(1) Yoffe, A. D. *Adv. Phys.* **1993**, *42*, 173.
(2) Berry, R. S. *Nature* **1998**, *393*, 212.
(3) Daniel, M.-C.; Astruc, D. *Chem. Rev.* **2004**, *104*, 293.
(4) Barnard, A. S.; Russo, S. P.; Snook, I. K. *J. Comput. Theor. Nanosci.* **2005**, *2*, 80.
(5) Harris, P. J. F. *Nature* (*London*) **1986**, *323*, 6091.
(6) Harris, P. J. F. *Surf. Sci.* **1987**, *185*, L459.
(7) Burda, C.; Chen, X.; Narayanan R.; El-Sayed, M. A. *Chem. Rev.* **2005**, *105*, 1025.
(8) Petrova, H.; Perez-Juste, J.; Zhang, Z.; Zhang, J.; Kosel, T.; Hartland, G. V. *J. Mater. Chem.* **2006**, *16*, 3957.
(9) Iacona, F.; Franzo, G.; Spinella, C. *J. Appl. Phys.* **2000**, *87*, 1295.
(10) Grom, G. F.; Lockwood, D. J.; McCaffrey, J. P.; et al. *Nature* **2000**, *407*, 358.
(11) Buhro, W. E.; Colvin, V. L. *Nat. Mater.* **2003**, *2*, 138.
(12) Barnard, A. S. *J. Mater. Chem.* **2006**, *16*, 813.
(13) Elechiguerra, J. L.; Reyes-Gasga, J.; José-Yacamán, M. *J. Mater. Chem.* **2006**, *16*, 3906.
(14) Pinto, A.; Pennisi, A. R.; Faraci, G.; D'Agostino, G.; Mobilio, S.; Boscherini, F. *Phys. Rev. B* **1995**, *51*, 5315.
(15) Bovin, J.-O.; Malm, J.-O. *Z. Phys. D* **1991**, *19*, 293.
(16) Buffat, P.-A.; Flüeli, M.; Spycher, R.; Stadelmann, P.; Borel, J.-P. *Faraday Discuss.* **1991**, *92*, 173.
(17) Ino, S.; *J. Phys. Soc. Jpn.* **1966**, *21*, 346. Ino, S.; Ogawa, S. *J. Phys. Soc. Jpn.* **1967**, *22*, 1365.
(18) Marks, L. D. *J. Cryst. Growth* **1983**, *61*, 556.
(19) Marks, L. D. *Rep. Prog. Phys.* **1994**, *57*, 603.
(20) Martin, T. P. *Phys. Rep.* **1996**, *273*, 199.
(21) Lisiecki, I.; Filankembo, A.; Sack-Kongehl, H.; Weiss, K.; Pileni, M. P.; Urban, J. *Phys. Rev. B* **2000**, *61*, 4968. Lisiecki, I.; Sack-Kongehl, H.; Weiss, K.; Urban J.; Pileni, M. P. *Langmuir* **2000**, *16*, 8802.
(22) Jana, N. R.; Gearheart, L.; Murphy, C. J. *Chem. Commun.* **2001**, 617.
(23) Sun, Y.; Xia, Y. *Adv. Mater.* **2002**, *14*, 833.
(24) Hu, J.-Q.; Chen, Q.; Xie, Z.-X.; Han, G.-B.; Wang, R.-H.; Ren, B.; Zhang, Y.; Yang, Z.-L.; Tian, Z.-Q. *Adv. Funct. Mater.* **2004**, *14*, 183.
(25) Liu, F.-K.; Huang, P.-W.; Chang, Y.-C.; Ko, C.-J.; Ko, F.-H.; Chu, T.-C. *J. Cryst. Growth* **2005**, *273*, 439.
(26) Wiley, B.; Sun, Y.; Mayers, B.; Xia, Y. *Chem.—Eur. J.* **2005**, *11*, 454.
(27) Harris, P. J. F. *Int. Mater. Rev.* **1995**, *40*, 97.
(28) Whetten, R. L.; Khoury, J. T.; Alvarez, M. M.; Murthy, S.; Vezmar, I.; Wang, Z. L.; Stephens, P. W.; Cleveland, C. L.; Luedtke, W. D.; Landman, U. *Adv. Mater.* **1996**, *8*, 428.
(29) Canizal, G.; Ascencio, J. A.; Gardea-Torresday, J.; José Yacamán, M. *J. Nanopart. Res.* **2001**, *3*, 475.
(30) José-Yacamán, M.; Ascencio, J. A.; Liu, H. B.; Gardea-Torresday, J. *J. Vac. Sci. Technol. B* **2001**, *19*, 1091.
(31) José-Yacamán, M.; Herrera, R.; Gómez, A. G.; Tehuacanero, S.; Schabes-Retchkiman, P. *Surf. Sci.* **1990**, *237*, 248.

(32) Häberlen, O. A.; Chung, S.-C.; Stener, M.; Rösch, N. *J. Chem. Phys.* **1997**, *106*, 5189.
(33) Cleveland, C. L.; Landman, U.; Schaaff, T. G.; Shafigullin, M. N.; Stephens, P. W.; Whetten, R. L. *Phys. Rev. Lett.* **1997**, *79*, 1873.
(34) Cleveland, C.; Luedtke, W. D.; Landman, U. *Phys. Rev. Lett.* **1998**, *81*, 2036.
(35) Ascencio, J. A.; Gutiérrez-Wing, C.; Espinosa, M. E.; Marin, M.; Tehuacanero, S.; Zorrilla, C.; José-Yacamán, M. *Surf. Sci.* **1998**, *396*, 349.
(36) Garzón, I. L.; Michaelian, K.; Beltrán, M. R.; Posada-Amarillas, A.; Ordejón, P.; Sánchez-Portal, D.; Soler, J. M. *Phys. Rev. Lett.* **1998**, *81*, 1600.
(37) Cleveland, C.; Luedtke, W. D.; Landman, U. *Phys. Rev. B* **1999**, *60*, 5065.
(38) Ascencio, J. A.; Perez, M.; José-Yacamán, M. *Surf. Sci.* **2000**, *447*, 73.
(39) Häkkinen, H.; Landman, U. *Phys. Rev. B* **2000**, *62*, R2287.
(40) Häkkinen, H.; Moseler, M.; Landman, U. *Phys. Rev. Lett.* **2002**, *89*, 033401.
(41) Wang, J. L.; Wang, G. H.; Zhao, J. J. *Phys. Rev. B* **2002**, *66*, 035418.
(42) Oviedo, J.; Palmer, R. E. *J. Chem. Phys.* **2002**, *117*, 9548.
(43) Gilb, S.; Weis, P.; Furche, F.; Ahlrichs, R.; Kappes, M. M. *J. Chem. Phys.* **2002**, *116*, 4094.
(44) Garzón, I. L.; Reyes-Nava, J. A.; Rodr×c1guez-Hernández, J. I.; Sigal, I.; Beltrán, M. R.; Michaelian, K. *Phys. Rev. B* **2002**, *66*, 073403.
(45) Nam, H.-S.; Hwang, N. M.; Yu, B. D.; Yoon, J.-K. *Phys. Rev. Lett.* **2002**, *89*, 275502.
(46) Baletto, F.; Ferrando, R.; Fortunelli, A.; Montalenti, F.; Mottet, C. *J. Chem. Phys.* **2005**, *77*, 3856.
(47) Zhao, J.; Yang, J.; Hou, J. G. *Phys. Rev. B* **2003**, *67*, 085404.
(48) Li, J.; Li, X.; Zhai, H.-J.; Wang, L.-S. *Science* **2003**, *299*, 964.
(49) Häkkinen, H.; Moseler, M.; Kostko, O.; Morgner, N.; Astruc Hoffman, M.; v. Issendorff, B. *Phys. Rev. Lett.* **2004**, *93*, 093401.
(50) Häkkinen, H.; Moseler, M. *Comput. Mater. Sci.* **2006**, *35*, 332.
(51) Barnard, A. S.; Curtiss, L. A. *ChemPhysChem* **2006**, *7*, 1544.
(52) O'Malley, B.; Snook, I. K. *Phys. Rev. Lett.* **2003**, *90*, 085702.
(53) Wulff, G. *Z. Kristallogr. Mineral.* **1901** *34*, 449.
(54) Ino, S. *J. Phys. Soc. Jpn.* **1969**, *27*, 941.
(55) Baletto, F.; Ferrando, R. *Rev. Mod. Phys.* **2005**, *77*, 371.
(56) Barnard, A. S.; Zapol, P. *J. Chem. Phys.* **2004**, *121*, 4276.
(57) Barnard, A. S.; Curtiss, L. A. *Rev. Adv. Mater. Sci.* **2005**, *10*, 105.
(58) Page, K.; Proffen, T.; Terrones, H.; Terrones, M.; Lee, L.; Yang, Y.; Stemmer, S.; Seshadri, R.; Cheetham, A. K. *Chem. Phys. Lett.* **2004**, *393*, 385.
(59) Barnard, A. S.; Lin, X. M.; Curtiss, L. A. *J. Phys. Chem. B* **2005**, *109*, 24465.
(60) Barnard, A. S.; Yeredla, R.; Xu, H. *Nanotechnology* **2006**, *17*, 3039.
(61) Saponjic, Z. V.; Dimitrijevic, N.; Tiede, D.; Goshe, A.; Zuo, X.; Chen, L.; Barnard, A. S.; Zapol, P.; Curtiss, L. A.; Rajh, T. *Adv. Mater.* **2004**, *17*, 965.
(62) Bapat, A.; Anderson, C.; Perrey, C. R.; Carter, C. B.; Campbell, S. A.; Kortshagen, U. *Plasma Phys. Controlled Fusion* **2004**, *46*, B97.
(63) Note that the total surface energy of a given nanocrystal is proportional to the total surface area (and increases slowly with size), while the total energy of the twin boundary is proportional to the total volume, and hence will increase more rapidly with the size.
(64) Rosengaard, N. M.; Skriver, H. L. *Phys. Rev. B* **1993**, *47*, 12865.
(65) Crampin, S.; Hampel, K.; Vvedensky, D. D.; Maclaren, J. M. *J. Mater. Res.* **1990**, *5*, 2107.
(66) Schweizer, S.; Elsässer, C.; Hummler, K.; Fähnle, M. *Phys. Rev. B* **1992**, *46*, 14270.
(67) Murr, L. E. *Scr. Metall.* **1972**, *6*, 203.
(68) Iijima, S.; Ichihashi, T. *Phys. Rev. Lett.* **1986**, *56*, 616.
(69) Kuo, C.-L.; Clancy, P. *J. Phys. Chem. B* **2005**, *109*, 13743.
(70) Baletto, F.; Mottet, C.; Ferrando, R. *Phys. Rev. Lett.* **2000**, *84*, 5544.
(71) Johnson, C. J.; Dujardin, E.; Davis, S. A.; Murphy, C.; Mann, S. *J. Mater. Chem.* **2002**, *12*, 1765.
(72) Jana, N. R.; Gearheart, L. A.; Obare, S. O.; Johnson, C. J.; Edler, K. J.; Mann, S.; Murphy, C. *J. Mater. Chem.* **2002**, *12*, 2909.
(73) Gao, J.; Bender, C. M.; Murphy, C. *Langmuir* **2003**, *19*, 9065.
(74) Chen, H. M.; Peng, H.-C.; Liu, R.-S.; Asakura, K.; Lee, C.-L.; Lee, J.-F.; Hu, S.-F. *J. Phys. Chem. B* **2005**, *109*, 19533.